Transmission and correlation of a two-photon pulse in a one-dimensional waveguide coupled with quantum emitters

Qingmei Hu, Bingsuo Zou, and Yongyou Zhang*
Beijing Key Lab of Nanophotonics & Ultrafine Optoelectronic Systems and School of Physics, Beijing Institute of Technology, Beijing 100081, China

(Received 25 November 2017; published 26 March 2018)

Transmission and correlation properties of a two-photon pulse are studied in a one-dimensional waveguide (1DW) in the presence of three types of quantum emitters: two-level atom (TLA), side optical cavity (SOC), and Jaynes-Cummings model (JCM). Since there are many plane-wave components for a two-photon pulse, a nonlinear waveguide dispersion is used instead of the linearized one. The two-photon transmission spectra become flatter with decreasing the pulse width. With respect to the δ coupling between the 1DW and quantum emitter the transmission dips show a blueshift for the non-δ one and the blueshift first increases and then decreases with increasing the width of the coupling. The TLA and JCM can induce an effective photon-photon interaction that depends on the distance between the two photons, while the SOC cannot. We show that the 1DW coupled with the TLA or JCM is able to evaluate the overlap of the two photons and that the non-δ coupling has potential for controlling the two-photon correlation.

DOI: 10.1103/PhysRevA.97.033847

I. INTRODUCTION

Operating single photons occupies an important position in quantum informatics [1–5], since as qubit carriers photons can transport fast and reliably over long distances or time [6]. One-dimensional waveguides (1DWs) coupled with quantum emitters provide a candidate for manipulating few-photon states [7–12]. Single-photon transportation was widely investigated in theory [13–19] and experiment [5,20–23]. Since there is no direct interaction between photons, it is a challenge to implement two-qubit gates [24,25], though they are necessary for operating quantum data encoded in photon states [26]. Remarkable attempts were made to address this difficulty by increasing nonlinearities at the level of individual photons [1,27,28]. One scheme is to use the 1DWs that are coupled with quantum emitters, such as two-level atoms (TLAs) [13,14,29–33], side optical cavities (SOCs) [34], or Jaynes-Cummings models (JCMs) [35–38]. The 1DWs cast by micro- and nanowires or line defects in photonic crystals confine photons to transport in one direction [21–23]. When the 1DW is coupled with quantum emitters, strong photon-emitter interaction opens an avenue for entanglement transfer [33], quantum networks [37], and other quantum devices. The quantum interference between the incident photon and that from the quantum emitters results in a complete single-photon reflection [39,40], multiphoton bound states [41–43], and photon clouds near quantum emitters [44–47]. Similar to the TLA, other atomlike objects such as quantum dots and superconducting qubits were also used due to their tunabilities [48–50]. Quantum electrodynamical systems of superconducting circuits [48,51] and optomechanical architectures [20,36,37] are typical applications for the 1DW coupled with the JCM with which the photon blockade effect [16,52] was observed. Moreover, a high-Q optical cavity coupled with quantum emitters can serve as a node in quantum networks [53].

Scattering dynamics of single-photon wave packets with ultranarrow bandwidth in the 1DWs can be studied by solving dynamical Schrödinger equations [34]. The TLA, SOC, and JCM show effectiveness for controlling the photon pulse in the 1DWs, such as waveform tailoring [54]. They also show strong influence on the transport of two-photon states, as well as the two-photon correlation [55]. We will focus on this topic in the present work, namely, the influence of the TLA, SOC, and JCM on the two-photon transmission and correlation in the 1DW. Compared with the single-photon case, the dynamics of the two-photon wave packets is much more complicated due to the two-photon correlation and nonlinearity of the TLA and JCM. For convenience we denote the quantum systems of the 1DWs that are coupled with the TLA, SOC, and JCM as 1DW-TLA, 1DW-SOC, and 1DW-JCM, respectively. For these three types of quantum systems most researchers adopted the δ function [34] to describe the coupling between the 1DW and quantum emitters. However, when the transverse size of the SOC is comparable to the wavelength of the incident light, the δ function is not available and thus the non-δ function should be used [56]. Existing methods for the two-photon scattering problem includes input-output [15,57], Lehmann-Symanzik-Zimmermann formalism [58,59], and the real-space formalism [34]. We use the real-space formalism to account for the non-δ coupling effects. A schematics for the 1DW non-δ coupled with a quantum emitter is given in Fig. 1, where the quantum emitter may be the TLA, SOC, or JCM. Their influences on the two-photon transmission and correlation are analyzed and compared mutually.

This work is organized as follows. In Sec. II we introduce the model and related formulas for the three quantum systems.

*Author to whom correspondence should be addressed: yyzhang@bit.edu.cn

Then, we discuss the two-photon transmission in Sec. III and two-photon correlation in Sec. IV. At last, a brief conclusion is summarized in Sec. V.

II. MODEL AND FORMULAS

The quantum system of the 1DW side coupled with a quantum emitter (see Fig. 1) is governed by the Hamiltonian

$$\mathcal{H} = \mathcal{H}_w + \mathcal{H}_e + \mathcal{H}_i. \tag{1}$$

$\mathcal{H}_w$ and $\mathcal{H}_e$ describe the waveguide and quantum emitter, respectively, and $\mathcal{H}_i$ corresponds to their interaction. $\mathcal{H}_w$ reads

$$\mathcal{H}_w = \sum_{\mu} \int dx \hat{\psi}_{\mu}^{\dagger}(x) \hat{\omega}_{\mu}(i\partial_x) \hat{\psi}_{\mu}(x), \tag{2}$$

where $\mu \in \{r, l\}$ denotes the right-/left-moving photon in the waveguide with the creation field $\hat{\psi}_{r/l}^{\dagger}(x)$ and energy operators $\hat{\omega}_{r/l}(i\partial_x)$. $\hat{\omega}_{\mu}(i\partial_x)$ is determined by the waveguide dispersion $\omega(k)$, i.e., $\hat{\omega}_{r/l}(i\partial_x) = \omega(-/+i\partial_x)$. We take

$$\omega(k) = \omega_0 \sqrt{1 + \left(\frac{k}{k_0}\right)^2}, \tag{3}$$

where ω_0 and k_0 measure the cut-off energy and lateral restraint of the waveguide. It represents the dispersion of a two-dimensional confined waveguide, such as a one-dimensional rectangular waveguide or a cylindrical waveguide. This dispersion gives a k-dependent group velocity,

$$v_g = \frac{\omega_0}{k_0} \frac{k}{k_0} \left(1 + \frac{k_0^2}{k^2}\right)^{-\frac{1}{2}}. \tag{4}$$

In most works $\omega(k)$ is linearized near the characteristic energies of the quantum emitter for simplicity, while this nonlinear dispersion is kept throughout the work. This is because the incident pulse we consider contains many plane-wave components, and the linearization approximation is not always valid. We assume that the quantum emitter has n modes and denote them as $\{|j\rangle\}$. Each mode with energy $\tilde{\omega}_j$ has a creation (annihilation) operator $\hat{\alpha}_j^{\dagger}$ ($\hat{\alpha}_j$), and thus $\mathcal{H}_e$ is a function of $\hat{\alpha}_j^{\dagger}$ and $\hat{\alpha}_j$, namely,

$$\mathcal{H}_e = \mathcal{H}_e(\{\alpha_j^{\dagger}\}, \{\alpha_j\}). \tag{5}$$

The interaction Hamiltonian $\mathcal{H}_i$ has the form

$$\mathcal{H}_i = \sum_{\mu, j} \int dx V_j(x) \hat{\psi}_{\mu}^{\dagger}(x) \hat{\alpha}_j + \text{H.c.}, \tag{6}$$

where $V_j(x)$ is the coupling strength between the photon field and quantum emitter mode $|j\rangle$.

We consider three types of quantum emitters: (i) TLA, (ii) SOC, and (iii) JCM. For the TLA only one excited state exists, that is, $\hat{\alpha}^{\dagger} = \hat{f}_e^{\dagger} \hat{f}_g$ and $\mathcal{H}_e = \tilde{\omega}_e \hat{f}_e^{\dagger} \hat{f}_e + \tilde{\omega}_g \hat{f}_g^{\dagger} \hat{f}_g$, where $\hat{f}_{g/e}^{\dagger}$ ($\hat{f}_{g/e}$) are the creation (annihilation) operators of the excited or ground electron with energies $\tilde{\omega}_{e/g}$. The coupling $V(x)$ is described by a δ function, i.e., $V(x) = V_0 \delta(x)$. Similar to the TLA we consider only one mode in the SOC for which $\hat{\alpha}^{\dagger} = \hat{c}^{\dagger}$ and $\mathcal{H}_e = \tilde{\omega}_c \hat{c}^{\dagger} \hat{c}$, where $\hat{c}^{\dagger}$ is the creation operator of the cavity photon. Since the SOC can have a large size along the waveguide, we adopt the Gaussian coupling

$$V(x) = V_0 \left(\frac{1}{4}\pi w^2\right)^{-1/2} e^{-4x^2/w^2}. \tag{7}$$

Its Fourier transform is $V_k = V_0 e^{-k^2 w^2/16}$. w measures the width of SOC and when $w \to 0$ $V(x)$ tends to $V_0 \delta(x)$. Because the JCM describes the coupling between one cavity (also a SOC) and one TLA, it has two modes described by $\hat{\alpha}_c^{\dagger} = \hat{c}^{\dagger}$ and $\hat{\alpha}_a^{\dagger} = \hat{f}_e^{\dagger} \hat{f}_g$ with $\mathcal{H}_e = \tilde{\omega}_e \hat{f}_e^{\dagger} \hat{f}_e + \tilde{\omega}_g \hat{f}_g^{\dagger} \hat{f}_g + \tilde{\omega}_c \hat{c}^{\dagger} \hat{c} + g(\hat{c}^{\dagger} \hat{f}_g^{\dagger} \hat{f}_e + \hat{f}_e^{\dagger} \hat{f}_g \hat{c})$. The subscript indices of c and a denote the cavity and atom, respectively, and g is the Rabi coupling. The coupling for the SOC with the waveguide is assumed to have the form in Eq. (7) and that for TLA with the waveguide is zero.

According to Eq. (1), the two-excitation state can be written out directly. We take the system of the 1DW-JCM as an example, whose two-excitation state is

$$\begin{aligned} |\Phi\rangle = & \sum_{\mu,\nu} \int dx_1 dx_2 \varphi_{\mu\nu}(x_1, x_2) \frac{1}{\sqrt{2}} \hat{\psi}_{\mu}^{\dagger}(x_1) \hat{\psi}_{\nu}^{\dagger}(x_2) |\varnothing\rangle \\ & + \sum_{\mu} \int dx \hat{\psi}_{\mu}^{\dagger}(x) [\varphi_{\mu c}(x) \hat{c}^{\dagger} + \varphi_{\mu a}(x) \hat{f}_e^{\dagger} \hat{f}_g] |\varnothing\rangle \\ & + C \frac{1}{\sqrt{2}} \hat{c}^{\dagger} \hat{c}^{\dagger} |\varnothing\rangle + A \hat{c}^{\dagger} \hat{f}_e^{\dagger} \hat{f}_g |\varnothing\rangle. \end{aligned} \tag{8}$$

Here, $|\varnothing\rangle$ is the vacuum state with the atom in the ground state and no photon in the system, and $\varphi_{\mu\nu}(x_1, x_2)$ is the wave function of the two-photon state and meets the permutation symmetry $\varphi_{\mu\nu}(x_1, x_2) = \varphi_{\nu\mu}(x_2, x_1)$. $\varphi_{\mu j}(x)$ implies that one excitation is in the waveguide and another is in $|j\rangle$. C and A represent the amplitudes of the two-excitation states $\hat{c}^{\dagger} \hat{c}^{\dagger} |\varnothing\rangle$ and $\hat{c}^{\dagger} \hat{f}_e^{\dagger} \hat{f}_g |\varnothing\rangle$, respectively. Substituting Eqs. (1) and (8) into the Schrödinger equation,

$$i\hbar \frac{\partial}{\partial t} |\Phi\rangle = \mathcal{H} |\Phi\rangle, \tag{9}$$

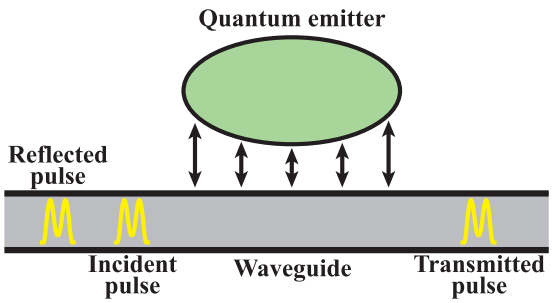

FIG. 1. Schematics of a waveguide side coupled with a quantum emitter. The yellow curves represent a two-photon pulse in the waveguide whose non-δ coupling with the quantum emitter is denoted by black arrows. The quantum emitter considered may be the TLA, SOC, or JCM.

gives the coupled dynamical equations for $\varphi_{\mu\nu}(x_1,x_2)$, $\varphi_{\mu c}(x)$, $\varphi_{\mu a}(x)$, C, and A as follows:

$$i\frac{\partial}{\partial t}\varphi_{\mu\nu}(x_1,x_2) = [\hat{\omega}_\mu(i\partial_{x_1}) + \hat{\omega}_\nu(i\partial_{x_2})]\varphi_{\mu\nu}(x_1,x_2) + \frac{\sqrt{2}}{2}[V(x_1)\varphi_{\nu c}(x_2)+V(x_2)\varphi_{\mu c}(x_1)], \quad (10a)$$

$$i\frac{\partial}{\partial t}\varphi_{\mu c}(x) = [\hat{\omega}_\mu(i\partial_x) + \tilde{\omega}_c]\varphi_{\mu c}(x) + \sqrt{2}V(x)C + g\varphi_{\mu a}(x) + \sqrt{2}\int dx' V^*(x')[\varphi_{\mu\mu}(x,x') + \varphi_{\mu\bar{\mu}}(x,x')], \quad (10b)$$

$$i\frac{\partial}{\partial t}\varphi_{\mu a}(x) = [\hat{\omega}_\mu(i\partial_x) + \tilde{\omega}_a]\varphi_{\mu a}(x) + V(x)A + g\varphi_{\mu c}(x), \quad (10c)$$

$$i\frac{\partial}{\partial t}C = 2\tilde{\omega}_c C + \sqrt{2}\sum_\mu \int dx V^*(x)\varphi_{\mu c}(x) + \sqrt{2}gA, \quad (10d)$$

$$i\frac{\partial}{\partial t}A = (\tilde{\omega}_c + \tilde{\omega}_a)A + \sum_\mu \int dx V^*(x)\varphi_{\mu a}(x) + \sqrt{2}gC, \quad (10e)$$

where $\bar{\mu} = r$ (l) if $\mu = l$ (r). The dynamical equations for the system of the 1DW-SOC can be obtained by setting $g = 0$, $A = 0$, and $\varphi_{\mu a} = 0$, while for the system of the 1DW-TLA one should first set $g = 0$, $A = 0$, $\varphi_{\mu a} = 0$, and $C = 0$, and then make the transform of $\varphi_{\mu c} \to \varphi_{\mu a}$. In the map for the 1DW-TLA, the setting of $C = 0$ ensures the resulting TLA cannot be in a double-excitation state [refer to Eq. (8)]. Because the nonlinear dispersion in Eq. (3) is taken for the 1DW, it is convenient to work in the reciprocal space and so we do a Fourier transform for Eq. (10), i.e.,

$$i\frac{\partial}{\partial t}\varphi_{\mu\nu}(k_1,k_2) = [\omega_\mu(k_1) + \omega_\nu(k_2)]\varphi_{\mu\nu}(k_1,k_2) + \frac{\sqrt{2}}{2}\left[V_{k_1}\varphi_{\nu c}(k_2) + V_{k_2}\varphi_{\mu c}(k_1)\right], \quad (11a)$$

$$i\frac{\partial}{\partial t}\varphi_{\mu c}(k) = [\omega_\mu(k) + \tilde{\omega}_c]\varphi_{\mu c}(k) + \sqrt{2}V_k C + g\varphi_{\mu a}(k) + \sqrt{2}\int dk' V_{k'}[\varphi_{\mu\mu}(k,k') + \varphi_{\mu\bar{\mu}}(k,k')], \quad (11b)$$

$$i\frac{\partial}{\partial t}\varphi_{\mu a}(k) = [\omega_\mu(k) + \tilde{\omega}_a]\varphi_{\mu a}(k) + V_k A + g\varphi_{\mu c}(k), \quad (11c)$$

$$i\frac{\partial}{\partial t}C = 2\tilde{\omega}_c C + \sqrt{2}\sum_\mu \int dk V_k\varphi_{\mu c}(k) + \sqrt{2}gA, \quad (11d)$$

$$i\frac{\partial}{\partial t}A = (\tilde{\omega}_c + \tilde{\omega}_a)A + \sum_\mu \int dx V_k\varphi_{\mu a}(k) + \sqrt{2}gC, \quad (11e)$$

where the equation of $V_{-k} = V_k$ is used. The Fourier transformations for $\varphi_{\mu\nu}(x_1,x_2)$, $\varphi_{\mu c}(x)$, and $\varphi_{\mu a}(x)$ are

$$\varphi_{\mu\nu}(k_1,k_2) = \frac{1}{2\pi}\int dk_1 dk_2 \varphi_{\mu\nu}(x_1,x_2)e^{is_\mu k_1 x_1 + is_\nu k_2 x_2}, \quad (12a)$$

$$\varphi_{\mu c}(k) = \frac{1}{\sqrt{2\pi}}\int dk \varphi_{\mu c}(x)e^{is_\mu kx}, \quad (12b)$$

$$\varphi_{\mu a}(k) = \frac{1}{\sqrt{2\pi}}\int dk \varphi_{\mu a}(x)e^{is_\mu kx}, \quad (12c)$$

where $s_\mu = +/-$ if $\mu = r/l$.

Once the wave functions are found from Eq. (10), the densities for the right- and left-moving photons, $\rho_{r/l}(x)$, can be obtained, namely,

$$\rho_\mu(x) = |\varphi_{\mu c}(x)|^2 + |\varphi_{\mu a}(x)|^2 + 2\int dx'[|\varphi_{\mu\mu}(x,x')|^2 + |\varphi_{\mu\bar{\mu}}(x,x')|^2], \quad (13)$$

and so the total photon density in the waveguide is $\rho_w(x) = \rho_r(x) + \rho_l(x)$. The factor 2 in Eq. (13) is due to the exchange symmetry in the two-photon states. Integrals of $\rho_{r/l}(x)$ give the numbers of the right- or left-moving photons,

$$n_\mu = \int dx \rho_\mu(x), \quad (14)$$

and the total number in the waveguide photons is

$$n_w = n_r + n_l. \quad (15)$$

When $t \to \infty$, $\frac{1}{2}n_r$ and $\frac{1}{2}n_l$ measure the transmission and reflection of the system, respectively. The excitation numbers in the SOC and TLA, respectively, are

$$n_c = \int dx'[|\varphi_{rc}(x)|^2 + |\varphi_{lc}(x)|^2] + 2|C|^2 + |A|^2 \quad (16)$$

$$n_a = \int dx'[|\varphi_{ra}(x)|^2 + |\varphi_{la}(x)|^2] + |A|^2. \quad (17)$$

The loss of the system reads

$$n_{\text{loss}} = 2 - (n_w + n_c + n_a). \quad (18)$$

The two-photon correlation can be described by the second-order correlation function, i.e.,

$$G^{(2)}_{x_1,x_2} = \langle\Phi|\hat{\psi}^\dagger(x_1)\hat{\psi}^\dagger(x_2)\hat{\psi}(x_2)\hat{\psi}(x_1)|\Phi\rangle = |\varphi_{rr}(x_1,x_2) + \varphi_{ll}(x_1,x_2) + \varphi_{rl}(x_1,x_2) + \varphi_{lr}(x_1,x_2)|^2, \quad (19)$$

where $\hat{\psi}(x) = \hat{\psi}_r(x) + \hat{\psi}_l(x)$. The second-order correlation function in the reciprocal space is given by

$$G^{(2)}_{k_1,k_2} = \int dx_1 dx_2 G^{(2)}_{x_1,x_2} e^{-ik_1x_1 - ik_2x_2}. \quad (20)$$

For solving the dynamical Eq. (10), one needs to choose an initial state which takes the following Gaussian type

throughout this work, i.e.,

$$\varphi_i(x_1,x_2) = \frac{1}{\sqrt{S}}[\phi(x_1 - x_{10})\phi(x_2 - x_{20}) + \phi(x_2 - x_{10})\phi(x_1 - x_{20})], \quad (21)$$

where $\phi(x) = e^{-\frac{1}{4}k_w^2 x^2} e^{ik_i x}$ and $S = \int dx_1 dx_2 |\varphi_i(x_1,x_2)|^2$. x_{10} and x_{20} are the initial center positions of the two photons and their difference is denoted by $d = x_{20} - x_{10}$. k_w describes the width of the two-photon pulse ($\sim 2\sqrt{2}k_w^{-1}$), and k_i is the center wave vector corresponding to the energy $\varepsilon_i = \omega(k_i)$. $\varphi_i(x_1,x_2)$ meets the permutation symmetry, i.e., $\varphi_i(x_1,x_2) = \varphi_i(x_2,x_1)$.

In numerical calculation we take ω_0 and k_0 as the units of the energy and wave vectors, and the corresponding units for time and length are $\tau_0 = 2\pi/\omega_0$ and $\lambda_0 = 2\pi/k_0$. Other parameters adopted are as follows: for the SOC $\tilde{\omega}_c = \omega_c - i\gamma_c$ with the energy $\omega_c = 1.25\omega_0$ and the loss $\gamma_c = 0.01\omega_0$; for the TLA $\tilde{\omega}_g = 0$ and $\tilde{\omega}_e = \omega_a - i\gamma_a$ with the transition energy $\omega_a = 1.25\omega_0$ and the loss $\gamma_a = 0.001\omega_0$; the Rabi coupling $g = 0.1\omega_0$. In addition, we use the fourth-order Runge-Kutta and predictor-corrector methods to solve Eq. (11), discretized in the reciprocal space of $(0,4k_0) \times (0,4k_0)$ by the grid with $2^9 \times 2^9$ points. The numerical approach has been tested by comparing the single-photon transmission from our methods with that from the theory in Ref. [34].

III. TRANSMISSION

Figure 2 shows the time evolution of the two-photon pulse with $d = 0$ for the system of the 1DW-JCM, where the pulse is incident from the left direction. When it arrives at the position of the JCM (at $x = 0$), it is scattered [see Fig. 2(a)]. During the scattering process the incident photons have a chance to jump into the JCM, referred to the curves of n_c and n_a in Fig. 2(d). The losses of the cavity and atom are responsible for $n_{\rm loss} \neq 0$ after the scattering. Note that the nonlinear dispersion of the waveguide leads to a k-dependent v_g [see Eq. (4)]. As a result, the pulse shows a spread in space for large k_w [see Fig. 2(c)], while the spread is not obvious for small k_w [see Figs. 2(a) and 2(b)]. The width of the pulse in Eq. (21) is $\sim 2\sqrt{2}k_w^{-1}$ and is $\sqrt{2}k_0[(\varepsilon_i/\omega_0)^2 - 1]^{1/2}/\pi k_w$ times its center wavelength. For $\varepsilon_i = \omega_c = 1.25\omega_0$ the multiple is $\sim$6.8, 3.4, and 2.3 when $k_w = 0.05k_0$, $0.1k_0$, and $0.15k_0$, respectively. Therefore, when the pulse width is in magnitude of its wavelength, the linearization for the 1DW dispersion $\omega(k)$ is not a good approximation, while when the pulse width is 5 times larger than the wavelength it can be adopted for simplicity.

Another main effect for increasing k_w is to smooth the transmission spectra, shown in Fig. 3 where the transmissivity for the three quantum systems are all plotted. As k_w increases the transmission curves become flatter, especially around the minimum or maximum points. For the TLA and SOC there is only one transmission dip, while for the JCM there are

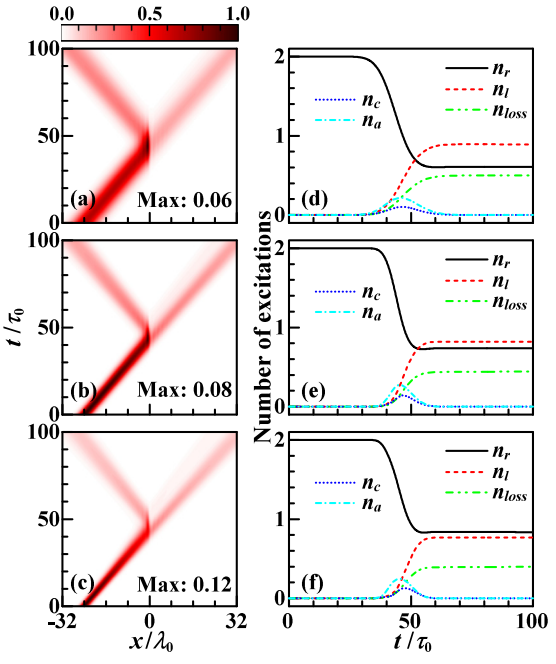

FIG. 2. Time evolution of the waveguide photon density (a)–(c) and of the corresponding number of excitations (d)–(f) for the 1DW-JCM. The width of the two-photon pulse in k space is set to $k_w = 0.05k_0$ (a), (d), $0.1k_0$ (b), (e), and $0.15k_0$ (c), (f), respectively. For easy observation, the photon densities in (a)–(c) are normalized to their maximum (see the bottom of the panels). Other parameters: $\omega_a = \omega_c = 1.25\omega_0$, $\gamma_c = 10^{-2}\omega_0$, $\gamma_a = 10^{-3}\omega_0$, $g = 0.1\omega_0$, $V_0 = 0.1\omega_0$, $w = 0.3\lambda_0$, $k_i = 0.65k_0$, and $d = 0$.

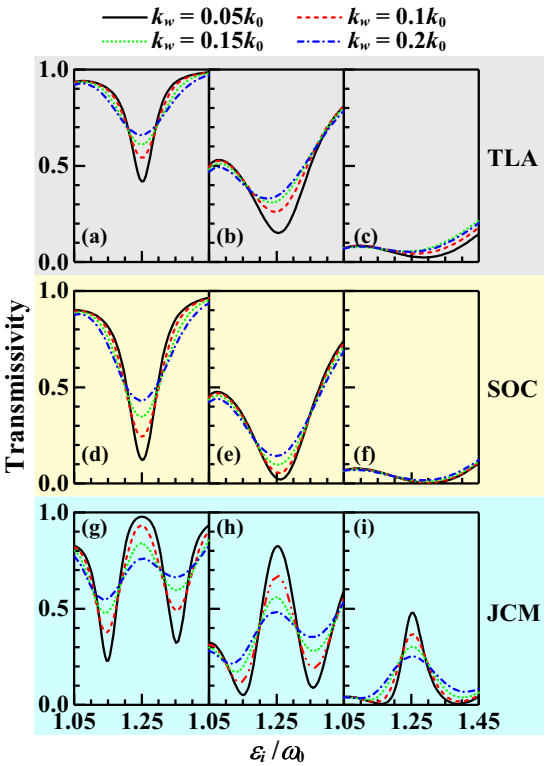

FIG. 3. Transmissivity of two-photon states for the 1DW-TLA (upper row), 1DW-SOC (middle row), and 1DW-JCM (lower row). The coupling constant $V_0/\lambda_0^{1/2}$ equals $0.05\omega_0$, $0.1\omega_0$, and $0.2\omega_0$ for columns from left to right. Other parameters: $\omega_a = \omega_c = 1.25\omega_0$, $\gamma_c = 10^{-2}\omega_0$, $\gamma_a = 10^{-3}\omega_0$, $g = 0.1\omega_0$, $w = 0$, and $d = 0$.

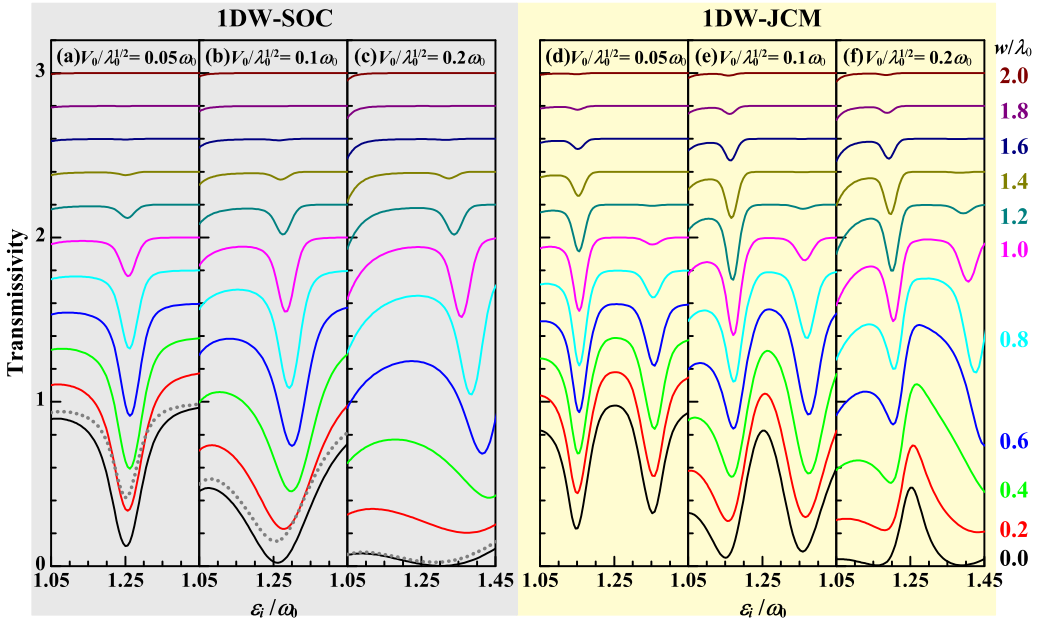

FIG. 4. Variation of transmission spectra with the width w of $V(x)$ for the 1DW-SOC (left gray panel) and 1DW-JCM (right yellow panel). The value of w for each curve is given on the right side of the figure and V_0 is at the top of each panel. The dotted curves in panels (a)–(c) are the transmission spectra of the 1DW-TLA whose coupling with the 1DW is set to $V(x) = V_0\delta(x)$. For easy observation, lines are offset from the bottom with a step value of 0.5. Other parameters: $\omega_a = \omega_c = 1.25\omega_0$, $\gamma_c = 10^{-2}\omega_0$, $\gamma_a = 10^{-3}\omega_0$, $g = 0.1\omega_0$, $d = 0$, and $k_w = 0.05k_0$.

two, because their mode numbers are different. In analogy to the single-photon transmission, one can introduce an effective coupling between the 1DW and SOC, i.e., $J = \frac{V_0^2}{v_g}$. Since J is an increasing function of V_0, resulting in the transmission decrease for increasing V_0, see the curves in columns from left to right. In addition, J shows an inverse function relationship with v_g, and v_g decreases with decreasing ε_i, so that the transmission spectra are nonsymmetric with respect to ω_c or ω_a, that is, the left side of the spectra is a little lower than the right (see Fig. 3). This fact also results in a rightward movement for the transmission dips, especially for large V_0 [see Figs. 3(c), 3(f), and 3(i)]. Since Figs. 2 and 3 tell that the approximation of the linearization of $\omega(k)$ is not suitable for a narrow pulse input, the nonlinearity of $\omega(k)$ is considered in all the numerical calculation throughout this work.

In Figs. 2 and 3 the coupling function $V(x)$ is taken as a δ function, i.e., $V(x) = V_0\delta(x)$, which is a good description for the local point coupling between the 1DW and quantum emitter, while for a large SOC its coupling with the 1DW is mainly determined by the SOC mode and thus can be other types of functions. The non-δ coupling effect on the transmission of the two-photon state is shown in Fig. 4 for the 1DW-SOC and 1DW-JCM. Because there is no effective interaction between two photons in the 1DW-SOC, the transmission of the two-photon state is similar with that of the single-photon state [56]. For example, Fig. 4(a) shows that the transmission dips are always on the right side of ω_c, implying that the frequency of the hybridization mode between the 1DW and SOC is blueshifted. Further, the blueshift value first increases and then decreases with increasing w, because the transmission dip first shifts rightward and then leftward with increasing w. This variation behavior of the transmission dip is enhanced by increasing V_0 [see Figs. 4(b) and 4(c)], and the transmission dip is broadened simultaneously. For a non-δ coupling function the effective coupling between the 1DW and SOC can be defined as $J_k = \frac{V_k^2}{v_g}$, where V_k, the Fourier transform of $V(x)$, decreases with increasing w. As a result, the transmission dip becomes shallower for increasing w.

The dotted gray curves in Figs. 4(a)–4(c) represent the transmission spectra of the 1DW-TLA where $w = 0$, corresponding to the δ coupling between the 1DW and TLA. Similar to the 1DW-SOC, the transmission of the 1DW-TLA decreases with increasing V_0, as shown in Fig. 3. The transmission dip is shallower for the 1DW-TLA than the 1DW-SOC [see the dotted gray and solid black lines in Figs. 4(a)–4(c)], though the single-photon transmission in them is consistent with each other. This can be argued as follows: Double occupation is forbidden in the TLA, so that the TLA cannot fully antiresonantly scatter the two-photon state, while the SOC can because it has the double-occupation state. The TLA does not influence the transport of the second photon if it has been excited by the first one (that is, the TLA cannot be excited twice).

Combining the TLA and SOC, one gets the JCM whose transmission spectra are also plotted as a function of w in Figs. 4(d)–4(f). The transmission spectra have two transmission dips, corresponding to the energy levels of the JCM that are about $1.15\omega_0$ and $1.35\omega_0$. The difference between two levels is $2g$. Similar to the 1DW-SOC, the two transmission dips first shift rightward and then leftward with increasing w, which can also be enhanced by increasing V_0. The transparent region between the two transmission dips exhibits a very narrow spectrum when g is small, analogous to electromagnetically induced transparency phenomena. Since v_g increases for increasing the photon energy, the local minimum is smaller for the left transmission dip than the right one. As a result, the right transmission dip disappears sooner than the left

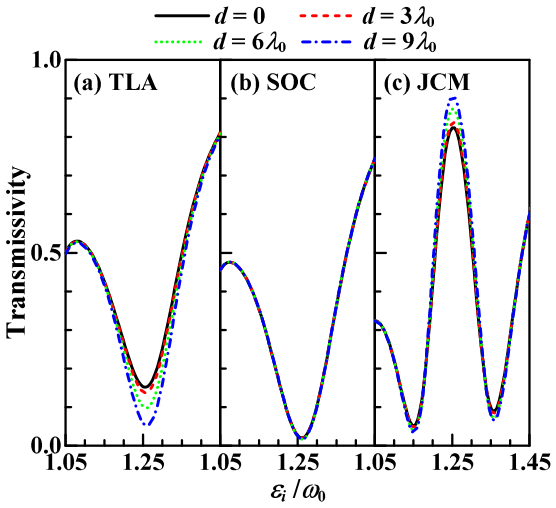

FIG. 5. Variation of transmission spectra with distance d between the two incident photons for the 1DW-TLA (left), 1DW-SOC (middle), and 1DW-JCM (right). Other parameters: $\omega_a = \omega_c = 1.25\omega_0$, $\gamma_c = 10^{-2}\omega_0$, $\gamma_a = 10^{-3}\omega_0$, $g = 0.1\omega_0$, $V_0 = 0.1\omega_0$, $k_w = 0.05k_0$, and $w = 0$.

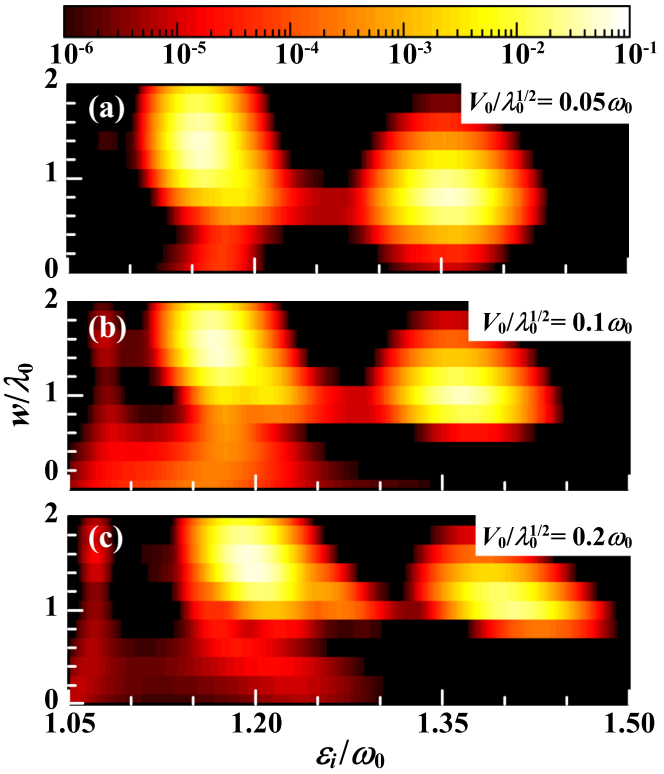

FIG. 6. Variation of $n_a|_{t\to\infty}$ with the width w of $V(x)$ and incident energy ε_i for the 1DW-JCM. Other parameters: $\omega_a = \omega_c = 1.25\omega_0$, $\gamma_c = \gamma_a = 0$, $g = 0.1\omega_0$, $k_w = 0.05k_0$, and $w = 0$.

when w increases [see Figs. 4(d)–4(f)]. This can also be confirmed by comparing the 1DW-JCM with the 1DW-SOC. The transmission dip in the 1DW-SOC disappears sooner than the left one in the 1DW-JCM but later than the right one. In all, the nonlinear dispersion and non-δ coupling provide more abundance for the transmission of the two-photon pulse.

The transmission of the two-photon pulse also shows strong dependence on the distance d between the two incident photons (see Fig. 5). For the 1DW-TLA the local minimum around the transmission dip decreases with increasing d [see Fig. 5(a)]. The photon in the 1DW cannot be scattered by the TLA once it is excited. Since the two single-photon pulses described by $\phi(x - x_{10})$ and $\phi(x - x_{20})$ overlap heavily for small d [consequently, the two photons are indistinguishable, see Eq. (21)], the two-photon pulse comprised of them has large transmission. However, the two photons would be distinguishable when d is large enough. As a result, the transmission spectra of the two-photon state would tend to that of the single-photon pulse. Since the SOC has the double-occupation state, changing d does not influence the transmission spectra for the 1DW-SOC [see Fig. 5(b)]. As a combination of the TLA and SOC the transmission spectra of the 1DW-JCM are also dependent on d [see Fig. 5(c)], especially around the transmission peak and dips. This dependence can further be enhanced by increasing k_w, namely, decreasing the pulse width. Therefore, it is possible to evaluate the quality of the single-photon series by the 1DW-TLA and 1DW-JCM. When there is no overlap between any two single-photon states for a single-photon series, the local minimum around the transmission dip approaches zero, while it is nonzero.

In addition, the excitation number $n_a|_{t\to\infty}$ can identify the existence of the bound modes between the quantum emitters and waveguide photons [44–47]. These bound modes have an exponentially decaying photon "cloud" in the vicinity of the quantum emitters. Since the losses of the cavity and TLA always lead to $n_a|_{t\to\infty} = 0$ no matter whether the bound modes exist or not, we need to set γ_a and γ_c to be zero for the bound mode identification; see Fig. 6 where the 1DW-JCM is taken as an example to show the non-δ coupling effects on the bound modes. The excitation number $n_a|_{t\to\infty}$ has a nonzero value near the two transmission dips [refer to Figs. 4(d)–4(f)], indicating the existence of the bound modes. The excitation efficiency of the bound modes strongly depends on w; see Fig. 6(a) where, roughly speaking, $n_a|_{t\to\infty}$ first increases and then decreases with increasing w, which can be explained as follows. As $w \to 0$ the coupling between the waveguide and JCM appears only at a point (position of the JCM), that is, the photons that are not at this point in the waveguide have no chance to excite the JCM. Consequently, the excitation efficiency is small for small w. For large w as long as the photons are near the JCM, they have a chance to excite the JCM. Since V_k decreases with increasing w, the excitation efficiency becomes small again for large enough w. Furthermore, the fact that the effective coupling $J_k = \frac{V_k^2}{v_g}$ increases with decreasing v_g results in the nonzero value of $n_a|_{t\to\infty}$ in the low-ε_i region, especially for large V_0 [see Figs. 6(b) and 6(c)]. This is also why $n_a|_{t\to\infty}$ has larger values near the left than the right transmission dips.

IV. TWO-PHOTON CORRELATION

The scattering of the quantum emitters can induce a nontrivial correlation or entanglement between the two photons [55]. Figure 7 shows the two-photon correlations $G^{(2)}_{x_1,x_2}$ for three quantum systems with $V(x) = V_0\delta(x)$ under four different d.

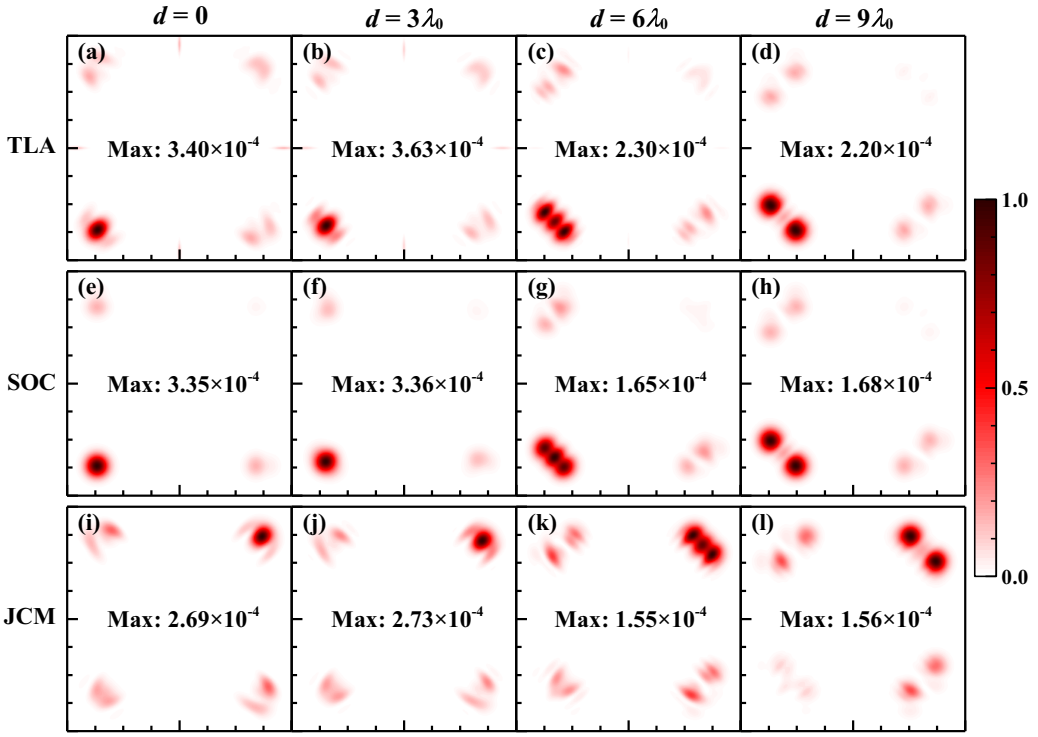

FIG. 7. Two-photon correlation after scattering for (a)–(d) TLA, (e)–(h) SOC, and (i)–(l) JCM in the real space ($80\lambda_0 \times 80\lambda_0$). For easy observation, the correlations in all panels are normalized to their maximums denoted by "Max." Each column has the same distance d which is given at the top. Other parameters: $\omega_a = \omega_c = 1.25\omega_0$, $\gamma_c = 10^{-2}\omega_0$, $\gamma_a = 10^{-3}\omega_0$, $g = 0.1\omega_0$, $k_w = 0.1k_0$, $k_i = 0.7k_0$, and $w = 0$.

The patterns in four corners of each panel correspond to the four waveguide photon wave functions, namely, the upper right to $\varphi_{rr}(x_1,x_2)$, lower right to $\varphi_{rl}(x_1,x_2)$, upper left to $\varphi_{lr}(x_1,x_2)$, and lower left to $\varphi_{ll}(x_1,x_2)$. Due to $\varphi_{\mu\nu}(x_1,x_2) = \varphi_{\nu\mu}(x_2,x_1)$ the two-photon correlation meets $G^{(2)}_{x_1,x_2} = G^{(2)}_{x_2,x_1}$, which is maintained by all panels in Fig. 7. When $d = 0$ the incident wave function $\varphi_i(x_1,x_2)$ is circularly symmetric in plane of x_1 and x_2. Since there is no effective interaction between the two photons in the 1DW-SOC, this circular symmetry is kept by the lower-left circular pattern in Fig. 7(e), corresponding to $\varphi_{ll}(x_1,x_2)$. However, for the 1DW-TLA and 1DW-JCM the circular symmetry is broken by the TLA-induced photon-photon interaction [see Figs. 7(a) and 7(i)]. Since there may exist a group delay for the transmitted and reflected waves [60], the distances from their packets to the quantum emitters are commonly different. In Fig. 7 the transmitted waves in the 1DW-TLA and 1DW-SOC and reflected waves in the 1DW-JCM are group delay. Consequently, when $d = 0$ the maximum values of $\varphi_{rl}(x_1,x_2)$ and $\varphi_{lr}(x_1,x_2)$ (one photon is transmitted and another is reflected) are not on the counterdiagonal lines of the panels, namely, not on the lines of $x_1 = -x_2$ [see Figs. 7(a), 7(e), and 7(i)]. On the contrary, the states of $\varphi_{rr}(x_1,x_2)$ and $\varphi_{ll}(x_1,x_2)$ have the maximum correlation when $x_1 = x_2$, because the two photons have the same delay or advancement. As d increases the two-photon correlations for the 1DW-TLA and 1DW-SOC become more and more similar [see Figs. 7(a)–7(h)]. It is also because the overlapping between the two photons decreases for increasing d and so does their mutual effective interaction. A similar variation behavior for the mutual influence between the two photons can be found for the 1DW-JCM, though its two-photon correlation pattern does not look like those in the 1DW-TLA and 1DW-SOC, which can be seen more obviously in the reciprocal space.

The two-photon correlations in the reciprocal space, namely, $G^{(2)}_{k_1,k_2}$, are shown in Fig. 8 where the panels correspond to those in Fig. 7 one-to-one. The main difference among the patterns in Fig. 8 is that when d is small there is a scatter ring for the TLA and JCM but not for the SOC. This is because the former two can induce an effective photon-photon interaction while the latter does not. The radius of the scatter ring is about $\sqrt{2}k_i = \sqrt{2} \times 0.7k_0 \approx 0.99k_0$, which is determined by the energy conservation. The energy conservation can be broken by the energy-time uncertainty during the scattering process, but here the two-photon correlation we are concerned with is far after the scattering process, i.e., the scattering has ended. According to Eq. (3) the scatter ring is determined by $2\sqrt{1+(k_i/k_0)^2} = \sqrt{1+(k_1/k_0)^2} + \sqrt{1+(k_2/k_0)^2}$, not a circle, strictly speaking. With increasing d the scatter ring gradually fades away because the effective photon-photon interaction decreases. Since the TLA takes over only part of the JCM, the effective photon-photon interaction induced by the JCM is weaker than that induced by the TLA (see the first and third rows in Fig. 8).

When d is large enough the two-photon transmission spectra for three quantum systems gradually tend to their single-photon transmission spectra. Since there exist transmission dips at the eigenfrequencies of the quantum emitters, the two-photon correlation approaches zero at the eigenfrequencies, as denoted by "TD" in Figs. 8(d), 8(h), and 8(l). The corresponding wave vectors are $0.75k_0$ for the TLA and SOC and are $0.57k_0$ and $0.9k_0$ for the JCM. Since there is a transmission peak for the JCM between the two transmission dips, the

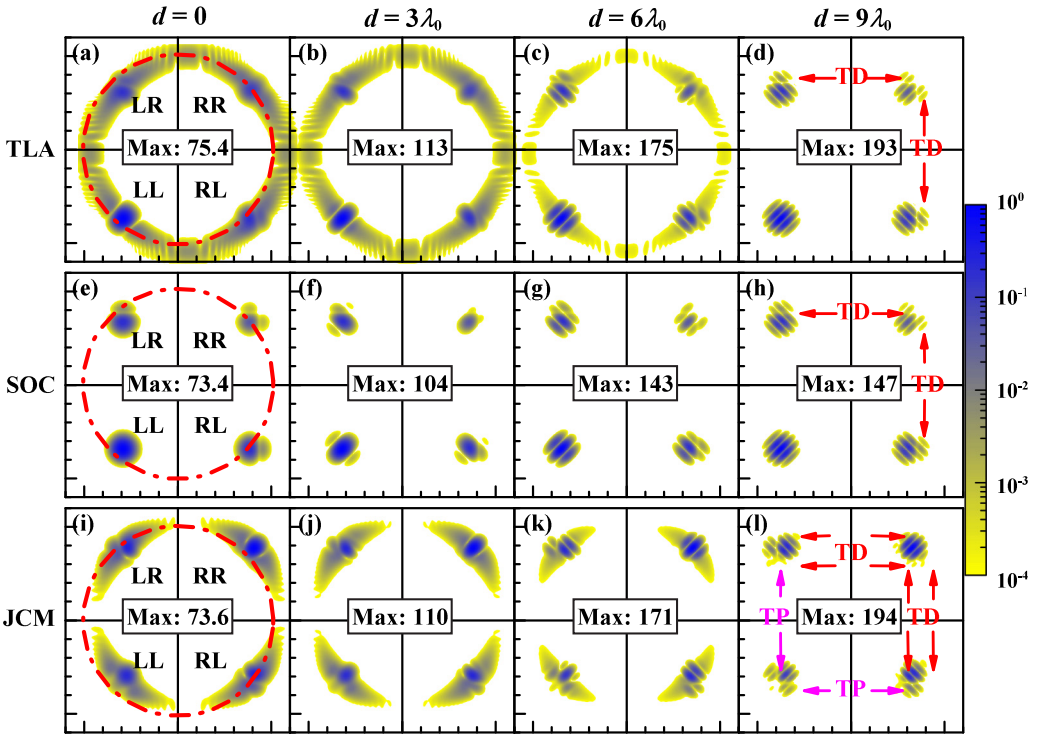

FIG. 8. Two-photon correlation after scattering for (a)–(d) TLA, (e)–(h) SOC, and (i)–(l) JCM in the reciprocal space ($2.4k_0 \times 2.4k_0$). The panels (a)–(l) correspond to Figs. 7(a)–7(l), respectively. The denotations of "RR," "RL," "LR," and "LL" correspond to the states of φ_{rr}, φ_{rl}, φ_{lr}, and φ_{ll}, respectively. "TD" and "TP" represent the transmission dip and peak, respectively. Other indication and parameters are the same as those in Fig. 7.

two-photon correlation also approaches zero at the position of the transmission peak, i.e., $0.75k_0$, denoted by "TP" in Fig. 8(l). Without ambiguousness the lines denoted by "TD" and "TP" can be called zero-correlation lines. Obviously, these zero-correlation lines always exist for the SOC no matter the value of d [see Figs. 8(e)–8(h)]. On the contrary, due to the effective photon-photon interaction they disappear for the TLA and JCM when d takes small values [see Figs. 8(a)–8(d) and 8(i)–8(l)]. These phenomena confirm that the TLA can really induce an effective photon-photon interaction and the SOC cannot. As a result, the TLA and JCM can induce the scatter ring for the two-photon state.

Figure 9 shows the two-photon correlation after scattering for the JCM in the real and reciprocal spaces with the non-δ coupling between the cavity and 1DW. In the real space the two-photon correlation for the non-δ coupling is similar

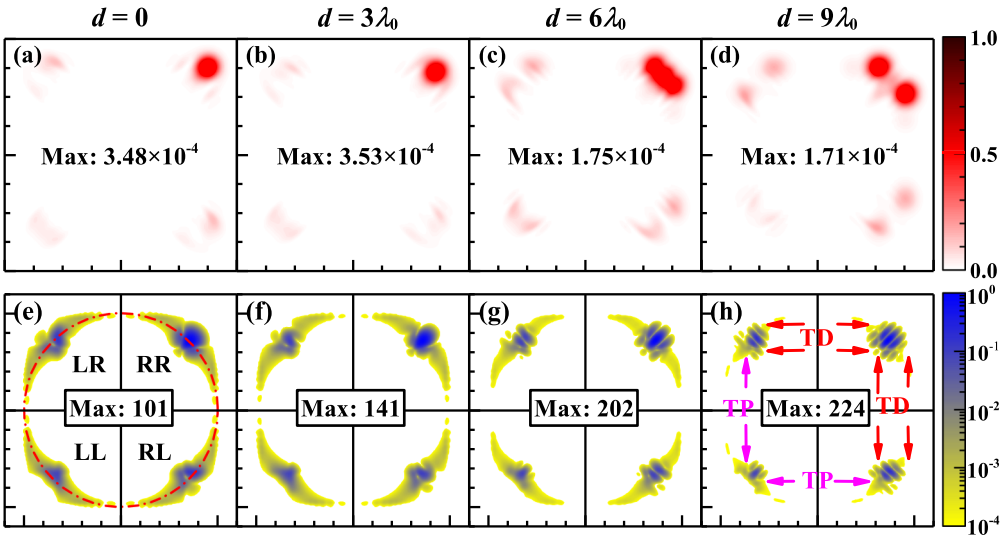

FIG. 9. Two-photon correlation after scattering for the JCM in (a)–(d) the real space ($80\lambda_0 \times 80\lambda_0$) and (e)–(h) the reciprocal space ($2.4k_0 \times 2.4k_0$). Other indications and parameters are the same as those in Figs. 7 and 8, except $w = 0.6\lambda_0$.

to that for the δ coupling, comparing Figs. 9(a)–9(d) with Figs. 7(i)–7(l), respectively. However, in the reciprocal space the two-photon correlations show an obvious difference in Figs. 9(e)–9(h) as compared with Figs. 8(i)–8(l). The amplitude of the non-δ coupling function, i.e., $V_k = V_0 e^{-k^2 w^2/16}$ with $w = 0.6\lambda_0$, is not larger than that of the δ coupling function, i.e., $V_k = V_0$, so that the scatter rings for the non-δ coupling become more slender but have a longer tail [compare Figs. 9(e)–9(h) with Figs. 8(i)–8(l)]. The long tail occurs because the non-δ coupling can connect two more-distant photons with respect to the δ coupling. In addition, the transmission dips for the JCM are blueshifted for the non-δ coupling, and so do the zero-correlation lines in Fig. 9(h). From the numerical results, we find that their corresponding wave vectors are $0.62k_0$ and $0.94k_0$ for the transmission dips and $0.76k_0$ for the transmission peaks when $w = 0.6\lambda_0$. Therefore, the non-δ coupling between the cavity and 1DW shows potential for controlling the correlation between two distant photons.

V. CONCLUSION

The transmission and correlation properties of the two-photon pulse were studied in the 1DW coupled with the TLA, SOC, and JCM. For the TLA the coupling is a δ type, while for the SOC and JCM the coupling can be non-δ type. Since a pulse contains many plane-wave components, a nonlinear waveguide dispersion is used instead of the linear one. Comparing with the δ coupling the non-δ coupling is able to induce a blueshift for the transmission dips, and the blueshift value first increases and then decreases for increasing the coupling width. When the pulse width in the reciprocal space increases, the two-photon transmission becomes flatter and flatter because more plane-wave components are included. Since a double occupation is forbidden in the TLA, the TLA cannot fully antiresonantly scatter the two-photon state, while the SOC can because it has the double-occupation state. The two-photon correlations were also studied in the real and reciprocal spaces. A scatter ring can be observed for the 1DW-TLA and 1DW-JCM, while it cannot for the SOC. Different from the SOC, the TLA and JCM can induce an effective photon-photon interaction. With increasing the distance between the two incident photons the scatter ring fades away. The transmission dips and transmission peaks are responsible for the zero-correlation lines on the scatter rings. By the effective interaction induced by the 1DW-TLA and 1DW-JCM they can be used to evaluate the overlap of the two incident photons. As a result, it may be possible to evaluate the single-photon series by the 1DW-TLA and 1DW-JCM. In addition, the non-δ coupling between the quantum emitter and 1DW shows potential for controlling the two-photon correlation.

ACKNOWLEDGMENTS

This work is supported by the NSFC (Grant No. 11304015) and the Beijing Higher Education Young Elite Teacher Project (Grant No. YETP1228).

[1] C. Santori, D. Fattal, J. Vuckovic, G. S. Solomon, and Y. Yamamoto, Nature (London) **419**, 594 (2002).
[2] J. L. O'Brien, A. Furusawa, and J. Vuckovic, Nat. Photonics **3**, 687 (2009).
[3] M. E. Reimer, G. Bulgarini, N. Akopian, M. Hocevar, M. B. Bavinck, M. A. Verheijen, E. P. A. M. Bakkers, L. P. Kouwenhoven, and V. Zwiller, Nat. Commun. **3**, 737 (2012).
[4] C. Eichler, D. Bozyigit, C. Lang, L. Steffen, J. Fink, and A. Wallraff, Phys. Rev. Lett. **106**, 220503 (2011).
[5] A. Laucht, S. Putz, T. Gunthner, N. Hauke, R. Saive, S. Frederick, M. Bichler, M. C. Amann, A. W. Holleitner, M. Kaniber, and J. J. Finley, Phys. Rev. X **2**, 011014 (2012).
[6] Q.-C. Sun, Y.-F. Jiang, Y.-L. Mao, L.-X. You, W. Zhang, W.-J. Zhang, X. Jiang, T.-Y. Chen, H. Li, Y.-D. Huang, X.-F. Chen, Z. Wang, J. Fan, Q. Zhang, and J.-W. Pan, Optica **4**, 1214 (2017).
[7] J. T. Shen and S. Fan, Phys. Rev. Lett. **98**, 153003 (2007).
[8] L. Zhou, S. Yang, Y. X. Liu, C. P. Sun, and F. Nori, Phys. Rev. A **80**, 062109 (2009).
[9] H. Dong, Z. R. Gong, H. Ian, L. Zhou, and C. P. Sun, Phys. Rev. A **79**, 063847 (2009).
[10] P. Longo, P. Schmitteckert, and K. Busch, Phys. Rev. Lett. **104**, 023602 (2010).
[11] D. Roy, Phys. Rev. Lett. **106**, 053601 (2011).
[12] Z. L. Ji and S. Y. Gao, Opt. Commun. **285**, 1302 (2012).
[13] J. T. Shen and S. Fan, Opt. Lett. **30**, 2001 (2005).
[14] L. Zhou, Z. R. Gong, Y. X. Liu, C. P. Sun, and F. Nori, Phys. Rev. Lett. **101**, 100501 (2008).
[15] S. Fan, S. E. Kocabas, and J. T. Shen, Phys. Rev. A **82**, 063821 (2010).
[16] J. F. Huang, J. Q. Liao, and C. P. Sun, Phys. Rev. A **87**, 023822 (2013).
[17] C. Martens, P. Longo, and K. Busch, New J. Phys. **15**, 083019 (2013).
[18] H. Zheng and H. U. Baranger, Phys. Rev. Lett. **110**, 113601 (2013).
[19] D. Roy and N. Bondyopadhaya, Phys. Rev. A **89**, 043806 (2014).
[20] B. Dayan, A. S. Parkins, T. Aoki, E. P. Ostby, K. J. Vahala, and H. J. Kimble, Science **319**, 1062 (2008).
[21] M. Bajcsy, S. Hofferberth, V. Balic, T. Peyronel, M. Hafezi, A. S. Zibrov, V. Vuletic, and M. D. Lukin, Phys. Rev. Lett. **102**, 203902 (2009).
[22] J. Bleuse, J. Claudon, M. Creasey, N. S. Malik, J. M. Gérard, I. Maksymov, J.-P. Hugonin, and P. Lalanne, Phys. Rev. Lett. **106**, 103601 (2011).
[23] I. C. Hoi, C. M. Wilson, G. Johansson, T. Palomaki, B. Peropadre, and P. Delsing, Phys. Rev. Lett. **107**, 073601 (2011).
[24] E. Knill, R. Laflamme, and G. J. Milburn, Nature (London) **409**, 46 (2001).
[25] P. Kok, W. J. Munro, K. Nemoto, T. C. Ralph, J. P. Dowling, and G. J. Milburn, Rev. Mod. Phys. **79**, 135 (2007).
[26] T. D. Ladd, F. Jelezko, R. Laflamme, Y. Nakamura, C. Monroe, and J. L. O'Brien, Nature (London) **464**, 45 (2010).
[27] U. Banin, Y. W. Cao, D. Katz, and O. Millo, Nature (London) **400**, 542 (1999).

[28] M. Bayer, O. Stern, P. Hawrylak, S. Fafard, and A. Forchel, Nature (London) **405**, 923 (2000).
[29] J. T. Shen and S. Fan, Phys. Rev. A **76**, 062709 (2007).
[30] X. F. Zang and C. Jiang, J. Phys. B **43**, 215501 (2010).
[31] J. Lu, L. Zhou, H. C. Fu, and L. M. Kuang, Phys. Rev. A **81**, 062111 (2010).
[32] M. T. Cheng, Y. Y. Song, Y. Q. Luo, and G. X. Zhao, Commun. Theor. Phys. **55**, 501 (2011).
[33] A. Gonzalez-Tudela, D. Martin-Cano, E. Moreno, L. Martin-Moreno, C. Tejedor, and F. J. Garcia-Vidal, Phys. Rev. Lett. **106**, 020501 (2011).
[34] J.-T. Shen and S. Fan, Phys. Rev. A **79**, 023837 (2009).
[35] L. M. Duan and H. J. Kimble, Phys. Rev. Lett. **92**, 127902 (2004).
[36] K. Srinivasan and O. Painter, Nature (London) **450**, 862 (2007).
[37] H. J. Kimble, Nature (London) **453**, 1023 (2008).
[38] K. Koshino, S. Ishizaka, and Y. Nakamura, Phys. Rev. A **82**, 010301 (2010).
[39] J. T. Shen and S. Fan, Phys. Rev. Lett. **95**, 213001 (2005).
[40] A. Auffeves-Garnier, C. Simon, J. M. Gerard, and J. P. Poizat, Phys. Rev. A **75**, 053823 (2007).
[41] R. Y. Chiao, I. H. Deutsch, and J. C. Garrison, Phys. Rev. Lett. **67**, 1399 (1991).
[42] H. X. Zheng, D. J. Gauthier, and H. U. Baranger, Phys. Rev. A **82**, 063816 (2010).
[43] C. Z. Zhu, S. Endo, P. Naidon, and P. Zhang, Few-Body Syst. **54**, 1921 (2013).
[44] J. S. Douglas, H. Habibian, C. L. Hung, A. V. Gorshkov, H. J. Kimble, and D. E. Chang, Nat. Photonics **9**, 326 (2015).
[45] G. Calajó, F. Ciccarello, D. Chang, and P. Rabl, Phys. Rev. A **93**, 033833 (2016).
[46] T. Shi, Y.-H. Wu, A. González-Tudela, and J. I. Cirac, Phys. Rev. X **6**, 021027 (2016).
[47] Ş. E. Kocabaş, Phys. Rev. A **93**, 033829 (2016).
[48] A. Wallraff, D. I. Schuster, A. Blais, L. Frunzio, R. Huang, J. Majer, S. Kumar, S. M. Girvin, and R. J. Schoelkopf, Nature (London) **431**, 162 (2004).
[49] A. V. Akimov, A. Mukherjee, C. L. Yu, D. E. Chang, A. S. Zibrov, P. R. Hemmer, H. Park, and M. D. Lukin, Nature (London) **450**, 402 (2007).
[50] J. M. Gambetta, A. A. Houck, and A. Blais, Phys. Rev. Lett. **106**, 030502 (2011).
[51] L.-J. Jin, M. Houzet, J. S. Meyer, H. U. Baranger, and F. W. J. Hekking, Phys. Rev. B **92**, 134503 (2015).
[52] K. M. Birnbaum, A. Boca, R. Miller, A. D. Boozer, T. E. Northup, and H. J. Kimble, Nature (London) **436**, 87 (2005).
[53] J. I. Cirac, P. Zoller, H. J. Kimble, and H. Mabuchi, Phys. Rev. Lett. **78**, 3221 (1997).
[54] Y. Wang, Y. Zhang, Q. Zhang, B. Zou, and U. Schwingenschlogl, Sci. Rep. **6**, 33867 (2016).
[55] A. Nysteen, P. T. Kristensen, D. P. S. McCutcheon, P. Kaer, and J. Mork, New J. Phys. **17**, 023030 (2015).
[56] Y. Zhang and B. Zou, Phys. Rev. A **89**, 063815 (2014).
[57] C. W. Gardiner and M. J. Collett, Phys. Rev. A **31**, 3761 (1985).
[58] T. Shi and C. P. Sun, Phys. Rev. B **79**, 205111 (2009).
[59] T. Shi, S. Fan, and C. P. Sun, Phys. Rev. A **84**, 063803 (2011).
[60] G. D. Dong, Y. Y. Zhang, M. A. Kamran, and B. S. Zou, J. Appl. Phys. **113**, 143105 (2013).